Int J CARS (2016) 11:667–678
DOI 10.1007/s11548-015-1297-8

ORIGINAL ARTICLE

Adaptive noise correction of dual-energy computed tomography images

Rafael Simon Maia[1] · Christian Jacob[1] · Amy K. Hara[2] · Alvin C. Silva[2] · William Pavlicek[2] · J. Ross Mitchell[2]

Received: 13 January 2015 / Accepted: 10 September 2015 / Published online: 13 October 2015

Abstract
Purpose Noise reduction in material density images is a necessary preprocessing step for the correct interpretation of dual-energy computed tomography (DECT) images. In this paper we describe a new method based on a local adaptive processing to reduce noise in DECT images
Methods An adaptive neighborhood Wiener (ANW) filter was implemented and customized to use local characteristics of material density images. The ANW filter employs a three-level wavelet approach, combined with the application of an anisotropic diffusion filter. Material density images and virtual monochromatic images are noise corrected with two resulting noise maps.
Results The algorithm was applied and quantitatively evaluated in a set of 36 images. From that set of images, three are shown here, and nine more are shown in the online supplementary material. Processed images had higher signal-to-noise ratio (SNR) and contrast-to-noise ratio (CNR) than the raw material density images. The average improvements in SNR and CNR for the material density images were 56.5 and 54.75 %, respectively.
Conclusion We developed a new DECT noise reduction algorithm. We demonstrate throughout a series of quantitative analyses that the algorithm improves the quality of material density images and virtual monochromatic images.

Keywords Material density · Dual-energy computed tomography · Noise reduction · Adaptive Wiener filter

Introduction

The usage of dual-energy computed tomography (DECT) in clinical settings is advantageous due to increased tissue discrimination properties obtained from the simultaneous acquisition of two linear attenuation images with different voltage settings. DECT can reduce the ambiguity inherent to the density and HU values obtained from regular computed tomography. Due to the acquisition of two linear attenuation images, it is possible to obtain extra physical information, which can be used to generate images that show material density information, effective atomic numbers, virtual monochromatic and virtual non-enhanced images that contribute to ameliorate image interpretation by the radiologist.

In the last three decades, many different technical solutions for the acquisition of DECT images have been attempted. Two of these technologies are currently mature and being sold commercially: the single-source rapid voltage switching approach by general electric (GE) and the dual-source approach by Siemens. Due to slightly different spectra, these two approaches have some intrinsic and important differences in the resulting images. While DECT does not have spectrographic qualities, the two basis material decomposition processes are flexible enough and capable of providing density information of many different pairs of basis materials, as long as their atomic numbers differ by at least 5. Unfortunately, that process results in images with significant

Electronic supplementary material The online version of this article (doi:10.1007/s11548-015-1297-8) contains supplementary material, which is available to authorized users.

✉ Rafael Simon Maia
rafaelsimonmaia@gmail.com

[1] Department of Computer Science, University of Calgary, 2500 University Dr NW, Calgary, AB T2N 1N4, Canada

[2] Department of Radiology, Mayo Clinic, 13400 E Shea Blvd, Scottsdale, AZ 85259, USA

more noise than in regular CT images. Since noisier images may negatively affect diagnoses, a preprocessing step that minimizes the noise is necessary.

In this paper, we explore the noise correction of material density images and virtual monochromatic images obtained from DECT data sets. Our technique takes into consideration both single- and dual-source scanners. It employs an adaptive neighborhood Wiener (ANW) filter to eliminate the noise in the material density images. The resulting noise maps can then be employed to correct the virtual monochromatic images at any energy level.

This paper is organized as follows: Second section describes related work. Third section quickly describes the Wiener filter. Fourth section describes our noise reduction algorithm. Fifth section presents the results, including an analysis of image quality. Discussion and Limitations of the present technique are discussed in sixth section. Finally, seventh section provides the conclusion and future work.

Related work

Dual-energy computed tomography is affected by the same noise artifacts that are found in regular CT. Therefore, most of the noise problems that affect the acquisition of a single linear attenuation image can be resolved with the same mature methods (for example, scanner calibration) that are applied to regular CT. Furthermore, it is known that noise-related errors that cause uncertainties in the measured attenuation values can be enhanced or decreased by an appropriate choice of image reconstruction algorithms and convolution kernels. Recently, the introduction of iterative and statistical reconstruction algorithms has provided radiologists with high-quality images, while, at the same time, decreasing [14] the total dose a patient is exposed to. However, they may increase the reconstruction time. More advanced reconstruction algorithms are still being actively investigated. In this paper, we limit this session to noise correction as a post-reconstruction step.

The problem of noise in DECT is more evident in images of derived information, as is the case with material density and virtual mono-chromatic images. Fortunately, Kalender et al. demonstrated [5] mathematically that noise in material density images is affected by negative correlation between the two different basis materials. They developed an algorithm that compensates for image degradation by using a simple mean filter and adding a noise correction map obtained from the first basis material image to the second basis material image. Their technique also attempts to keep the corrected values as close as possible to the original values. A similar technique was developed by Macovski et al. [8]. They combine a low-pass filter of the high-energy image and a high-pass filter of the low-energy image, to increase image quality of the virtual monochromatic images. Warp and Dobbins [16] have studied both techniques and concluded that they are mathematically related.

Hinshaw and Dobbins [4] have also focussed on the similar problem of noise correction of dual-energy radiography, developing algorithms that could be adapted to DECT. One of these algorithms, called noise clipping, restricts the pixel attenuation values within a range of low- and high-intensity values. A second technique, called noise forcing, examines the contrast between pixel values located in the foreground with those in the background. The difference between those values should decrease when going from the low-energy to the high-energy image. Consequently, pixels that violate this constraint are likely affected by noise.

An idea similar to Hinshaw and Dobbins' noise forcing technique is also seen in the spectral correction algorithm of Park et al. [10]. Their algorithm employs a three-step approach that first locates water pixels close to the zero Hounsfield units (HU) in both low- and high-energy images. Second, pixels that are identified as having increasing values, whereas their values should be decreasing, are swapped. As the third and last step, Kalender's technique is employed, resulting in final images with increased quality. In another work, Park et al. [11] attempted to use the Gram Schmidt orthonormalization process to remove noise from material density images. They assume that noise in the material density images is not only negatively correlated but also orthogonal to the vector space of the material basis. However, their results do not support such hypothesis. While the images appear to have better quality, the water density images suffer from cross-contamination from the iodine images, presenting values that appear to differ too much from the expected values.

Another recent technique reported by Grant et al. [3] uses a frequency-split approach to improve the quality of virtual monochromatic images obtained using Siemens dual-source scanners. They combine the lower spatial frequency stack of the low-energy linear attenuation image with the high spatial frequency of the monochromatic image obtained at the less noisy energy level (approximately 70 keV). The authors claim the technique improved the contrast while decreasing the noise in virtual monochromatic images. However, we have found that noise reduction improvements in the linear attenuation image space causes limited improvements in the material density images.

The application of anisotropic diffusion filters has been previously investigated in our own work [9] as well as in the works of Li et al. [7]. The diffusion equation and the main objectives of these papers differ. Li et al. focus on diminishing cross-contamination, while [7,9] attempt to preserve edges while simultaneously decreasing noise. The application of wavelets has also been investigated by Borsdorf et al. [2]. Their work is focused only on dual-source DECT; they

prefer to suppress the wavelet coefficients that are deemed correlated at each wavelet level of the linear attenuation image, which results in slight improvements in material density images.

A value-based approach was presented by Balda et al. [1]. Using a joint probability distribution of the linear attenuation values from both low- and high-energy images, they employ a gradient ascent algorithm that approximates the values of each pixel to the mean value of the pixel's main material. Finally, a comparison of post-reconstruction algorithms for noise correction of dual-energy radiography images is given by Warp and Dobbins [16].

Background: the Wiener filter

The Lee filter [6] is a good approximation of the Wiener filter using local image statistics. Its basic idea is to minimize the mean-square error estimation of the original image. In order to approximate local statistics, the Lee filter attempts to estimate the mean and variance necessary for its computation by using a square window with fixed size and fixed shape, centered on each pixel. Because of its fixed shape and size approach, the Lee filter suffers from poor noise filtering near the edges, especially when using large neighborhoods. At the same time, the Lee filter performs well in uniform areas. The Lee filter used here is formulated as:

$$\bar{f}(i,j) = \bar{g}(i,j) + \frac{v_g(i,j) + v_n(i,j)}{v_g(i,j)} \left(g(i,j) - \bar{g}(i,j)\right), \tag{1}$$

where $g(i,j)$ and $\bar{g}(i,j)$ are, respectively, the original image and the mean filtered version of the original image, $v_g(i,j)$ and $v_n(i,j)$ are, respectively, the variance of the original image and the variance of the noise, always estimated locally in a square window kernel of size $N \times N$.

Because the Lee filter uses local statistics that mostly ignore the size of uniform regions, as well as the presence of edges, it does not produce optimal results. Therefore, we adapt the Lee filter by using an adaptive neighborhood mean filter that was customized to take advantage of minimum noise linear attenuation in order to correct the material density images.

Methodology

Description of the algorithm

Contrary to the work of Balda et al. [1] and Borsdorf et al. [2], where linear attenuation or HU images are corrected first, our focus lies primarily on the noise correction of material density, followed by the correction of virtual monochromatic images in HU. The most common image size for CT images is 512×512 pixels. In order to tackle noise that may be larger than a pixel, we employed a multilevel Haar transform to reduce the image, which was applied three times, generating subimages of size 256, 128 and 64 square pixels. We have found that applying the Haar transform further generated no noticeable improvement in the final filtered image. We apply our ANW filter followed by an anisotropic diffusion filter at each wavelet level and again at the original image size. At each wavelet level, after the application of the Wiener filter and the anisotropic diffusion filter, we calculate an intermediate noise map by subtracting the filtered material density image from the original image, creating a correlated noise map and adding back a weighted version of that map to each material density image. In order to measure the level of image quality improvement achieved by the new algorithm and for comparison reasons, we also modify the algorithm, employing the classic Wiener filter in the form of the Lee filter instead of the newly proposed adaptive Wiener filter.

The adaptive Wiener filter

We modified the Lee filter so it employs an adaptive region growing method in its calculation of the mean value of a region. Instead of calculating the local statistics of noise and signal within a fixed window size and fixed window shaped local neighborhood (like in Fig. 1a), we employ an adaptive region growing technique that, given some constrains, finds an near-optimal, variable size and variable shape neighborhood (like in Fig. 1b) for each individual pixel in the image. This method was inspired by the work of Rangayyan et al. [13], who used a similar idea for natural images. We adapt and extend their idea to DECT material density images and take advantage of the edges obtained from the linear attenuation image with minimal noise to restrict growth in certain areas.

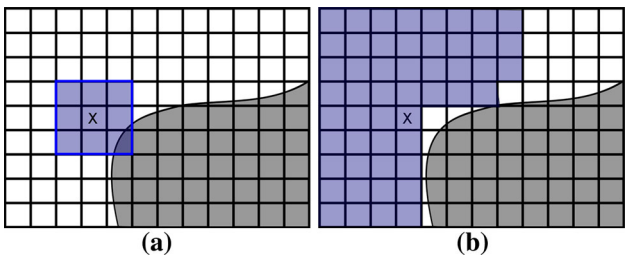

Fig. 1 **a** Usual 3×3 fixed size and fixed shape window over a region in a hypothetical image. **b** An region whose growth was limited by the existence of an edge and a distance of at most 4 pixels from the center pixel. The pixel marked with an *X* is the center pixel of both regions and will be updated with the mean value calculated from the pixels in each region. The mean pixel in (**a**) will be contaminated by including a pixel from the edge, while the center pixel in (**b**) will only be updated from pixels that are within the same uniform region. **a** Raw water density image. **b** Raw iodine density image

In our algorithm, in order to calculate the local statistics with an adaptive region, we first calculate the fixed size and fixed shape local mean and standard deviation of the image. We use a 3×3 pixel window and calculate the mean and standard deviation using MATLAB (The Math Works, Inc., Natick, MA, USA) *filter2* and *stdfilt* standard functions. Subsequently, we calculate the binary edges of the linear attenuation image with minimum noise, which is found around an energy level of 70 keVs [17]. We use the binary edge image to mark region boundaries, limiting the calculation of mean values in the marked regions to a window of 3×3 pixels. This means that the pixels marked as edges do not undergo region growing.

We mark the pixel locations of the edges in the linear attenuation image in both iodine and water density images. Although edges may not immediately be identifiable, we assume some edges do exist and are, in fact, hidden by noise. This fact is especially true for the iodine density images. The outer border of each image is treated without symmetric padding of values; therefore, the adaptive region grows only within the space of the original image. Since the boundaries of CT images are usually outside of the field of view, this does not affect the overall quality of the images.

A growing region will only include a new pixel if that pixel is not marked as a boundary. The pixel is only included if its value is within one standard deviation of the original mean value that was previously calculated with a 3×3 pixel window. If the new pixels in the current region are not within one standard deviation of the original mean value, they will be ignored and not taken into consideration for the updated mean and standard deviation calculations. If the pixels in the growing region are within that appropriated range, we calculate the new mean and the new standard deviation, updating those values accordingly.

The adaptive region used in the adaptive filter grows iteratively, but its maximum extent is limited to a square window of 13×13 pixels, which is approximately equal to $1\,\text{cm}^2$ in most images. This area property is also kept for each of the Haar transform levels, i.e., the maximum extent for the first wavelet level is 7×7 square pixels and so on. While this maximum extent value seems random, it was defined so that the region growing is locally limited and to avoid overly smoothing the image. This procedure is executed for all pixels, with the exception of the pixels that are within a region marked as being part of an edge. For the edge calculation we use a Sobel filter without thinning, in order to have the pixels that are relatively close to the true edge marked as edge pixels as well. The workflow describing the region growing procedure is detailed in Fig. 2.

The calculation of the final standard deviation values, which are required for the calculation of the variance in the Wiener filter, is left as the last step of the adaptive region growing mean filter. This step is necessary in order to ameliorate the standard deviation of the edge regions where the neighborhood was limited to a 3×3 neighborhood. One could be tempted to use the pure standard deviation of the final adaptive mean filter image. Yet we have found that this does not achieve optimal results, creating incorrect values when the Wiener filter is applied. Instead, we calculate the final standard deviation for the adaptive region growing mean filter image and for those pixels previously marked as edges. We update the final standard deviation by calculating the average between the original standard deviation (obtained from the material density image being corrected) and the standard deviation for the final adaptive mean filtered image.

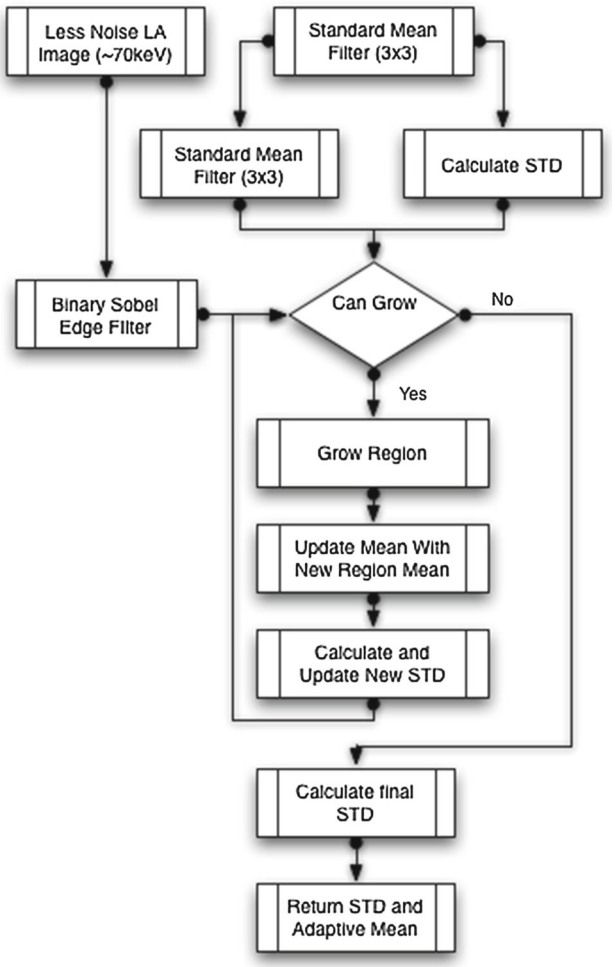

Fig. 2 Flowchart of the adaptive mean filter with region growing used in our algorithm

Anisotropic filter

By applying the adaptive Lee filter before the anisotropic diffusion filter, the intermediate image that will undergo the anisotropic diffusion filter will be much less noisy than before. Consequently, we have to adapt the noise estimation

function of our previous work, so that it is more sensitive to boundary conditions. We calculate the noise of each material density image individually and use the opposite material noise estimation as the gradient threshold function which is defined as:

$$\kappa = N + 2 \times \mu_m(70) \times Edges\left(\mu^{\mathrm{LA}}(70)\right), \tag{2}$$

where $\mu_m(70)$ is the linear attenuation value of a material m at the less noisy energy (70 keV), μ^{LA} is the linear attenuation image at the less noisy energy, which is found around the 70 keVs [17]. The function *Edges* calculates the edges of that image using the Prewitt filter [12]. Furthermore, N is defined as:

$$N = \frac{1}{\sqrt{2M^2}}\sqrt{im - G(im)}, \tag{3}$$

where G is a gaussian function and im is the current material density image being processed.

Noise map processing

The final step toward noise correction of the density images is the calculation of the temporary and final noise maps after the application of each wavelet transform, Wiener and anisotropic diffusion filter. For the current work, we modified the Algorithm A1 proposed by Kalender et al. [5], where he mathematically derived some of these values from the pre-reconstruction images. A combined temporary noise map C is calculated according to [5]:

$$C = 0.01 \times \mu_I^L(70) \times nm_i - \mu_M^L(70) \times nm_w \tag{4}$$

where nm_i and nm_w are the noise maps for iodine and water, respectively, obtained after the subtraction of the filtered image from its original version, at each scale, μ_I^L and μ_M^L are the linear attenuation values for iodine and water at 70 keV, respectively. The water noise map is obtained by weighting C by:

$$nm_W = \frac{1}{2 \times \mu_W^L} \times C, \tag{5}$$

where μ_M^L is the linear attenuation of water and C is the combined noise maps as defined in Eq. 4.

The noise map for iodine requires a few more calculations. We first need to estimate the noise using N (see Eq. 3). The values in N are normalized between 0 and 1 and then used to scale the gradient magnitude obtained applying a Sobel filter in the linear attenuation image at the keV with minimum noise, defined as:

$$E = \min(v, 1), \text{ with}$$
$$v = \frac{\left|sobel\left(\mu_{\mathrm{HU}}^L(70)\right)\right|}{N_W}, \tag{6}$$

where N_W is the noise for the water material density images, as defined in Eq. 3. The linear attenuation of the virtual monochromatic image is given by $\mu_{\mathrm{HU}}^L(70)$. The formula for the calculation of the noise map for iodine is then given by:

$$nm_I = 0.01 \times \left(1 - E^{2 \cdot N_W}\right) \times \mu_I^L(70) \times nm_W, \tag{7}$$

where the multiplication by 0.01 is used to put the resulting values in the correct unit.

The final noise maps can now be added back to the original material density images, as follows:

$$\rho_w^{\mathrm{NC}} = \rho_w^O + \left|\frac{-nm_w}{nm_I}\right| nm_I$$
$$\rho_I^{\mathrm{NC}} = \rho_I^O + \left(1 - \left|\frac{nm_I}{-nm_W}\right|\right) \times (-nm_W), \tag{8}$$

where ρ_w^O and ρ_I^O are the original material density images of water and iodine, respectively. The correction of virtual monochromatic CT images can be obtained by the modified Hounsfield units conversation, defined as [17]:

$$\mathrm{NC}(E) = \left(\frac{\mu_I^L(E)}{\mu_W^L(E)}\rho_I\right) + \left(\frac{\mu_I^L(70)}{\mu_W^L(70)} - \frac{\mu_I^L(E)}{\mu_W^L(E)}\right) \times nm_I$$
$$\mu^{\mathrm{HU}}(E) = \rho_W + 0.1 \times \mathrm{NC}(E) - 1000 \tag{9}$$

Quantitative measurement of image quality

In order to assess the improvement in terms of image quality, we chose to use a number of objective quantification measurements that can be obtained by evaluating certain mathematical attributes of the image. While subjective methods evaluated by a number of experts could provide a more realistic and correct estimation of quality, we opted to leave this as future work, instead focusing on classic quantitative methods.

We use two different types of quantitative measurements: (1) localized region of interest (ROI) and (2) ground truth comparisons using noiseless images obtained by simulation. We use both techniques to compare the image quality of the adaptive algorithm with that of the algorithm using the standard Wiener filter as well as with the original image. For the second case, our comparison is extended to a whole-image quantification approach using the noiseless simulated image as ground truth. For the ground truth comparison, we use a similarity metric that is based on an objective method for quality assessment based on the human visual system. This is done by using the structural similarity index metric (SSIM)

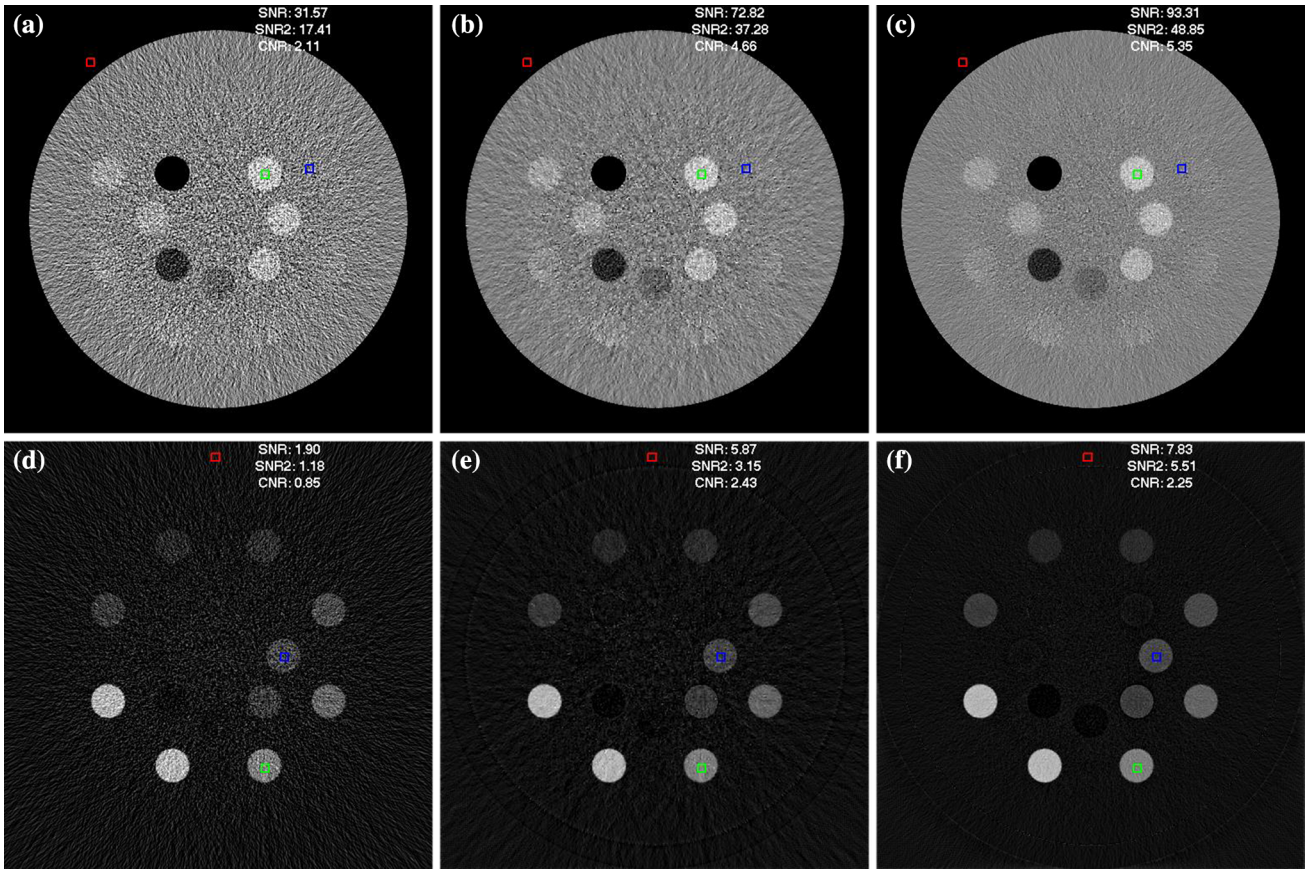

Fig. 3 Simulated Gammex 472 phantom scanned with the ImaSim CT simulation software. *Left column* contains the original images, *middle column* contains images corrected using the algorithm with the standard Wiener filter. *Third column* contains the images corrected with the algorithm using the adaptive Wiener filter. Average SNR gain was 66 % for water and 75 % for iodine density images. The CNR gain of 60 % for water and 62 % for iodine density image corrected using the adaptive filter when compared to the raw image. **a** Raw water image, **b** Wiener filtered water image, **c** adaptive Wiener filter water image, **d** raw iodine image, **e** Wiener filtered iodine image, **f** adaptive Wiener filter iodine image

described by Wang and Bovi [15]. The SSIM is used here to measure (1) how close an image obtained from the simulation with realistic (noisy) settings is compared to the corresponding image from the ideal simulation, and (2) whether there is any improvement in image quality after the noise reduction algorithms are applied.

Our measurements where done in images of simulated software phantoms (Gammex 472), physical phantom (Gammex 472) and real patient images. For the simulated phantom, we used ImaSim CT simulation software (version 1.0, Montreal, Canada) to create dual-energy scans of a virtual imitation of the physical Gammex 472. We acquired a set of simulations that contained no noise and were acquired using ImaSim's ideal integrator for ground truth reference. Another simulation was acquired with settings that were similar to those used in the image acquisition of the physical phantoms (350 and 550 mAs for 80 and 140 kVp, respectively) in order to approximate the same level of noise and artifacts observed in those images. The physical Gammex 472 phantom was scanned with both single- and dual-source techniques (GE and Siemens' scanners, respectively).

All water density images are shown with the same windowing setting, with a window center of 1000 and a window width of 300, representing a range of values between 850 and 1150. Similarly, all iodine density images are shown with the same window settings, with window center at 75 and window width of 87, representing a range of values from −12 to 172. CT images are shown in Hounsfield units, with window center at −250 and window width of 1000, resulting in a range of values from −1250 to 750.

ROI-based quantitative measurement of quality

Quantitative measurements of image quality who use regions of interest (ROI) usually examine a set of small regions in the image. These regions are usually chosen by an user by taking in consideration features like homogeneity and size. Noise in a homogenous region would be defined by the presence of

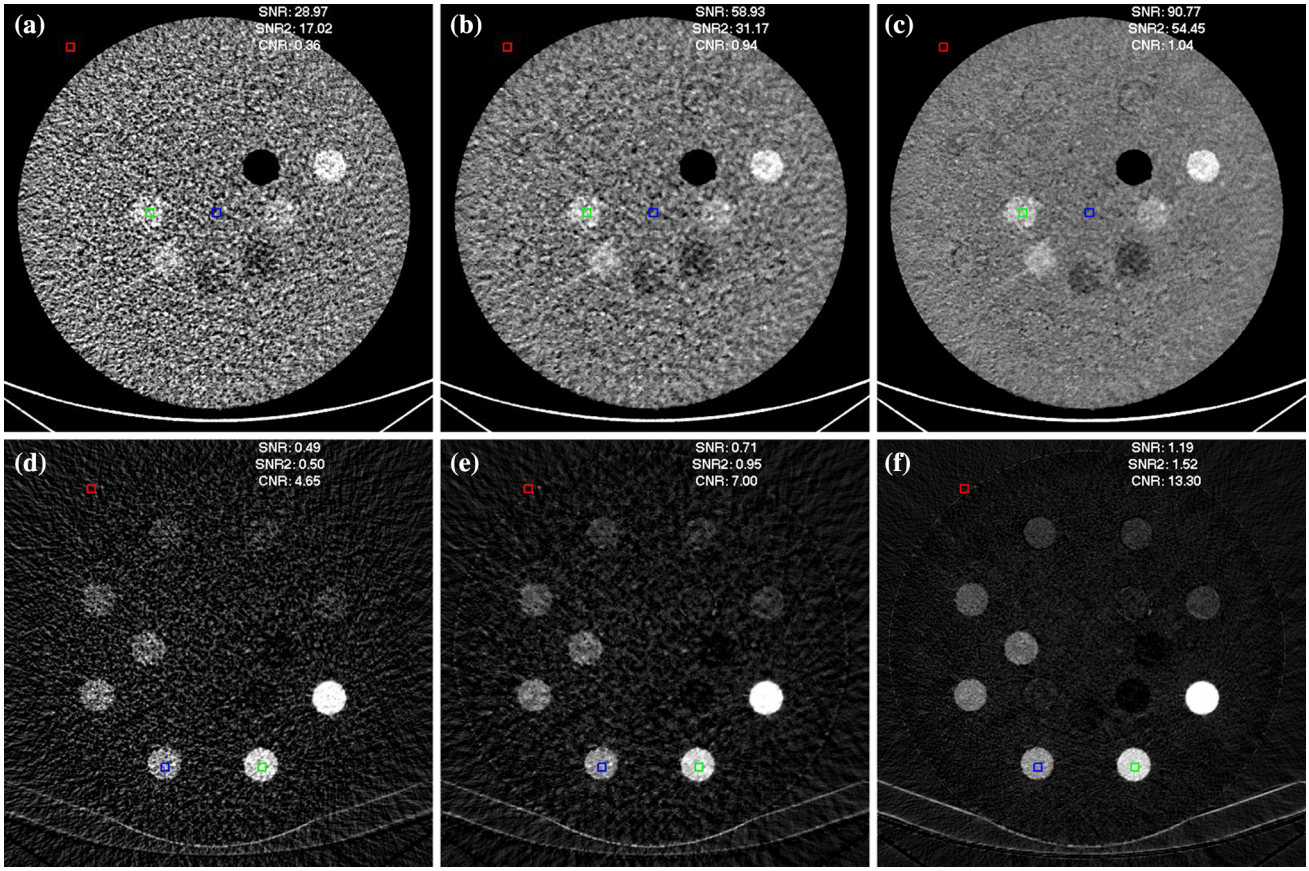

Fig. 4 Gammex 472 phantom scanned with a GE's single-source DECT Scanner. *Left column* contains original images, *middle column* contains images corrected using the algorithm with the standard Wiener filter. *Third column* shows images corrected with the algorithm using the adaptive Wiener filter. Average SNR gain was 68 % for water and 58 % for iodine density images. The CNR gain of 65 % for water and 65 % for iodine density images corrected using the adaptive filter when compared to the raw images. **a** Raw water image, **b** Wiener filtered water image, **c** adaptive Wiener filter water image, **d** raw iodine image, **e** Wiener filtered iodine image, **f** adaptive Wiener filter iodine image

a larger than expected standard deviation. The noise is more evident in the background (air) part of the image; therefore, its standard deviation is usually used for reference.

ROI-based measurements can be used to compare the differences in image quality between a pair of two images. In this paper, we use two kinds of measurements. The first kind, the signal-to-noise ratio (SNR), is measured in two different ways. The second kind of measurement is the contrast-to-noise ratio (CNR). The improvement or gain between each of the measurement is calculated from the original image in relation to its specific noise-corrected version. A positive value indicates some level of improvement, while a negative value some level of degradation. The first of these measurements, the SNR, will be defined as:

$$\mathrm{SNR} = \left|\frac{\mu_{\mathrm{foreground}}}{\sigma_{\mathrm{background}}}\right| \quad \text{or} \quad \mathrm{SNR2} = \left|\frac{\mu_{\mathrm{foreground}}}{\sigma_{\mathrm{foreground}}}\right| \tag{10}$$

where $\mu_{\mathrm{foreground}}$, $\sigma_{\mathrm{background}}$ and $\sigma_{\mathrm{foreground}}$ are the mean of the foreground, the standard deviation of the background and standard deviation of the foreground, respectively. The region of interest used in this paper is taken in regions of size 9×9 pixels. The improvement in terms of SNR between the filtered image and the original noisy image is then given by:

$$\mathrm{SNR}_{\mathrm{gain}} = 1 - \left(\frac{\mathrm{SNR}_{\mathrm{original}}}{\mathrm{SNR}_{\mathrm{corrected}}}\right) \times 100 \tag{11}$$

This equation can be applied to both types of SNR defined above. It returns a percentage value that demonstrates the local measurement gain in the filter image in relation to the same location in the original image. The CNR is defined as:

$$\mathrm{CNR} = \frac{|\mu_A - \mu_B|}{\sigma_{\mathrm{background}}} \tag{12}$$

where μ_A and μ_B are the mean values of two distinct regions of interest in the foreground of the image, while $\sigma_{\mathrm{background}}$ is the standard deviation of the background of the image. We define CNR gain following the same scheme seeing in Eq. 11.

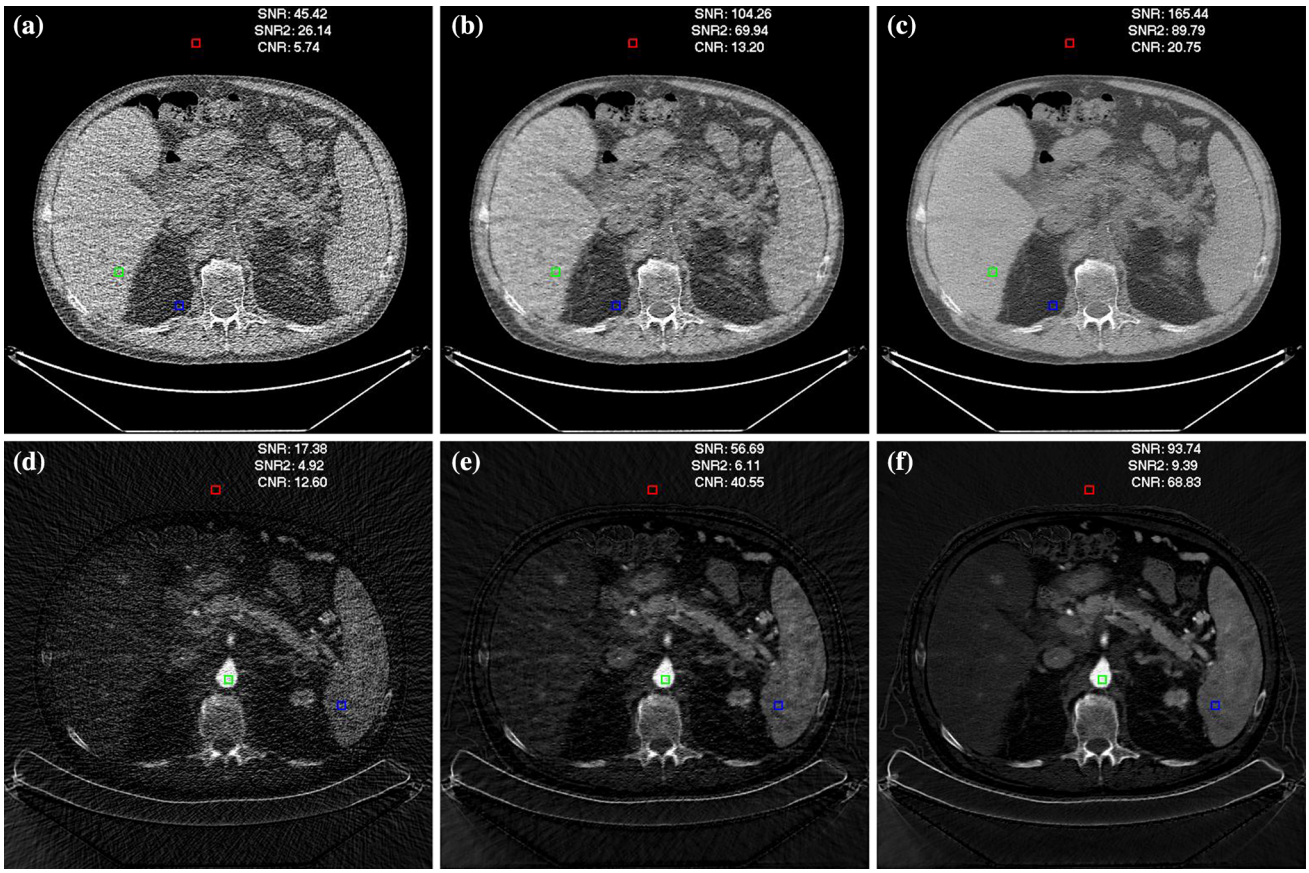

Fig. 5 Abdominal image acquired with a GE's single-source DECT Scanner. *Top column* shows original images, *second column* shows images corrected using the standard Wiener filter while *third column* contains the images using the ANW filter. Average SNR and SNR2 gain was 59 and 67 % respectively, with a CNR gain of 63 % for the adaptive filter when compared to the raw image. **a** Raw water image, **b** Wiener filtered water image, **c** adaptive Wiener filter water image, **d** raw iodine image, **e** Wiener filtered iodine image, **f** adaptive Wiener filter iodine image

Implementation

The prototype of our algorithm was implemented with MATLAB 2012b (The Math Works, Inc., Natick, MA, USA) using vectorized code whenever it was possible. The algorithm was then executed on a Mac Pro Early 2009 with an Intel Xeon Core of 3.5 GHz and 16 GB of RAM.

Results

The noise correction algorithm with the adaptive neighborhood Wiener filter, which was implemented in MATLAB, takes about 10 s to be executed for both pairs of material density images found in a single DECT slice. Given the constrains of the language and those of the region growing algorithm, it was not possible to take full advantage of the vectorization aspects of MATLAB, which contributed to the less then optimal performance. The algorithm with the standard Wiener filter performs slightly over a second for each pair of density images because it can take full advantage of vectorization. Nonetheless, the implementation of the adaptive algorithm in a massive processing language like OpenCL can be easily done and is left as future work.

In order to ascertain the usefulness of the algorithm in noise correcting the material density images obtained from single- and dual-source DECT, we used a Gammex 472 phantom with known amounts of different materials. The phantom was scanned by both GE (Discovery CT750) and Siemens (Somatom Definition) scanners. Furthermore, a simulated Gammex 472 phantom was modeled and scanned using ImaSim. Additionally, a set of other 33 slices of different body parts was also analyzed and some of the slices and other results are shown in the online supplementary material.

Material density images

We applied the adaptive neighborhood algorithm and the algorithm using the standard Wiener filter to a set of different images of increasing realism. Figure 3 shows a virtual Gam-

Table 1 SNR, SNR2 and CRN and relative improvements for the noise-reduced images over raw material density images

	SNR	SNR2	CNR	SNR gain (%)	SNR2 gain (%)	CNR gain (%)
Figure 3—water						
Raw water image	31.57	17.41	2.11			
Regular Wiener filtered water image	72.82	37.28	4.66	56.65	53.30	54.72
Adaptive Wiener filtered water image	93.31	48.85	5.35	66.17	64.36	60.56
Figure 3—iodine						
Raw iodine image	1.90	1.18	0.85			
Regular Wiener filtered iodine image	5.87	3.15	2.43	67.63	62.54	65.02
Adaptive Wiener filtered iodine image	7.83	5.51	2.25	75.73	78.58	62.22
Figure 4—water						
Raw water image	28.97	17.02	0.36			
Regular Wiener filtered water image	58.93	31.17	0.94	50.84	45.40	61.70
Adaptive Wiener filtered water image	90.77	54.45	1.04	68.08	68.74	65.38
Figure 4—iodine						
Raw iodine image	0.49	0.50	4.65			
Regular Wiener filtered iodine image	0.71	0.95	7.00	30.99	47.37	33.57
Adaptive Wiener filtered iodine image	1.19	1.52	13.30	58.82	67.11	65.04
Figure 5—water						
Raw water image	45.42	26.14	5.74			
Regular Wiener filtered water image	104.26	69.94	13.20	56.44	62.63	56.52
Adaptive Wiener filtered water image	165.44	89.79	20.75	72.55	70.89	72.34
Figure 5—iodine						
Raw iodine image	17.38	4.92	12.60			
Regular Wiener filtered iodine image	56.69	6.11	40.55	69.34	19.48	68.93
Adaptive Wiener filtered iodine image	93.74	9.39	68.83	81.46	47.60	81.69

SNR gain was close or higher to 60 % in most of the images examined

mex 472 phantom built using the simulator ImaSim. Images were scanned twice at different energies (80 and 140 kVp) and then underwent a two material decomposition processes in order to obtain the material density images for water and iodine. The average SNR gain was 66 % for water and 75 % for iodine density image and the CNR gain of 60 and 62 % for the adaptive filter when compared to the raw image. Figure 4 shows the results of applying the algorithm to the two material density images of an Gammex 472 phantom scanned with a GE scanner. A visual inspection of Figs. 3 and 4 shows that the adaptive algorithm performed similarly well in all three scans of the Gammex phantom, independently of the mechanism used to acquire the images and the settings used in the reconstruction step. Figure 5 shows a real patient abdominal image scanned with a GE scanner, which presents similar levels of quality improvements as previous. The improvement in terms of quantitative measurements for these figures is presented in Table 1, and it clearly shows the benefits of employing the adaptive Wiener filter for correcting material density images.

Additionally, Fig. 5 shows additional material density images from a patient slice. The statistics for those figure are also presented in Table 1. It is evident from both the quantitative and visual inspection of the material densities analyzed that the noise correction algorithm with the adaptive neighborhood Wiener filter provides much improved image quality. The behavior of the algorithm using the adaptive neighborhood Wiener filter is superior to that of the algorithm with the standard Wiener filter, for both SNR and CNR gains in all three kinds of acquisition techniques selected for the comparison.

Virtual monochromatic images

The image quality improvement in material density images is directly translated into improved virtual monochromatic HU images as well. Figure 6 shows the virtual monochromatic HU image (VMI) at 40 keV of Figs. 3, 4 and 5. Top images are the original VMI without noise correction, while bottom images show the noise-reduced VMI calculated using Eq. 10. The images with noise correction have evident better quality, and this is quantified in Table 2. The SNR and SNR2 gain is similar to what was shown for the monochromatic images, with an average improvement close or higher to 60 %. The

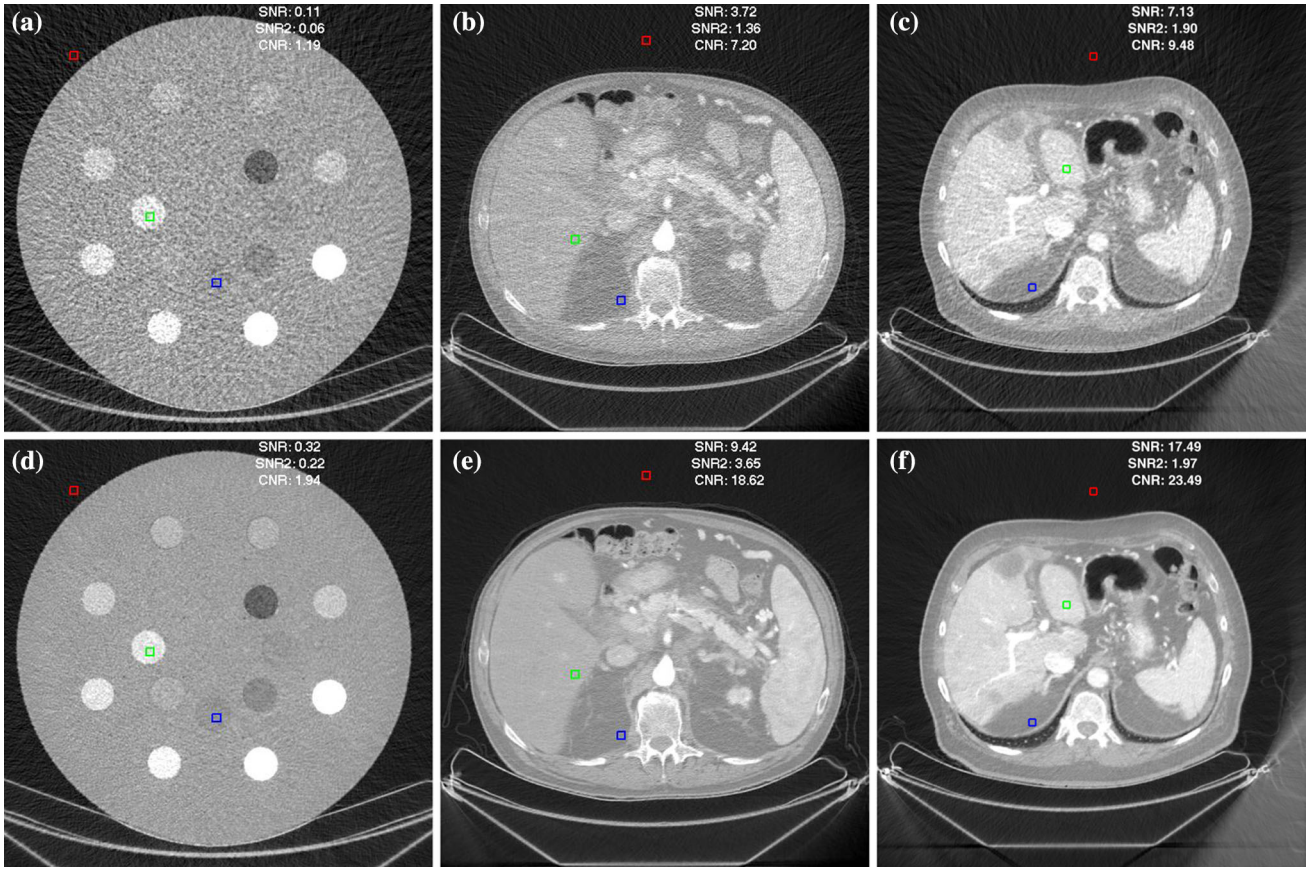

Fig. 6 Original and noise-reduced virtual monochromatic images at 40 keV of Figs. 4 and 5, in this order. *Top row* shows images generated without noise correction. *Bottom row* shows the images generated using the noise map obtained using the adaptive Wiener filter. The values are summarized in Table 2. **a** Raw VMI (40 keV) of Fig. 4, **b** raw VMI (40 keV) of Fig. 5, **c** raw VMI (40 keV) of Fig. 5, **d** filtered VMI (40 keV) of Fig. 4, **e** filtered VMI (40 keV) of Fig. 5, **f** filtered VMI (40 keV) of Fig. 5

Table 2 SNR, SNR2 and CRN and relative improvements for the noise-reduced VMI when compared to original raw images generated at 40 keVs

	SNR	SNR2	CNR	SNR gain (%)	SNR2 gain (%)	CNR gain (%)
Figure 4—VMI 40 keV						
Without noise correction	0.11	0.06	1.19			
Adaptive Wiener filtered	0.32	0.22	1.94	65.63	72.73	38.66
Figure 5—VMI 40 keV						
Without noise correction	3.72	1.36	7.20			
Adaptive Wiener filtered	9.42	3.65	18.62	60.51	62.74	61.33
Figure 6c—VMI 40 keV						
Without noise correction:	7.13	1.90	9.48			
Adaptive Wiener filtered:	17.49	1.97	23.49	59.23	3.55	59.64

Images corrected with the noise maps obtained after applying the algorithm with the adaptive Wiener filter show better image quality, with an average SNR gain higher than 60 % for the figures examined in this table

same improvement also happens for the CNR and is particularly noticeable in the images of the Gammex 472 phantom from Figs. 3 and 4. Additional images available in the supplementary material also show similar levels of SNR and CNR improvement.

Noise-reduced images present better defined edges, and the structures are more clearly visible than in the images without the application of the algorithm. The behavior of the algorithm is also approximately the same, independently of the mechanism of image acquisition used. The overall texture

and details present in the original image are also present in the noise-reduced images; however, due to the decrease in noise, they are much more visible.

Ground truth comparison using noiseless simulation

We used a CT simulation software called ImaSim, to create dual-energy scans of a virtual Gammex 472 phantom. We performed two scans of the virtual phantom that contained no noise (using ImaSim's ideal integrator) for ground truth reference and another set of dual-energy scans acquired with setting akin those used in the scanning of the real Gammex 472 using GE or Siemens scanners. The noiseless images are of very high quality and can be see in Fig. 7a, b. The realistic scans were obtained at 80 kVp (550 mAS) and 140 kVp (350 mAS) with standard filtering and detector of 1.04g mm of simulated ultra fast ceramic (Gd2O2S) detector. The realistic images can be see in Fig. 3. We compared the quality of the pair of noisy material density images with that of two pairs of noise-corrected density images. The first pair of material density images was corrected using the algorithm with the classic Wiener filter, while the second pair was corrected using the adaptive version of the algorithm. This two noise-corrected images can also be see in Fig. 3.

For the ground truth comparison, we use a similarity metric that is based on a objective method for quality assessment, which is based on the human visual system. This metric, called the structural similarity index, was developed by Wang and Bovik [15] and is used here to objectively measure how close the images obtained from simulation with realistic settings are to that of the ideal simulation, and whether there is any improvement between the realistic simulations after the noise reduction algorithms are applied. The structural similarity index of the images evaluated below is also presented as a scalar value in Table 3, which also corroborates the results obtained by visual inspections of structural similarity images shown in Fig. 7. By observing Fig. 7, we can objectively say that the adaptive Wiener filter approximates the noiseless image better than the algorithm using the classic Wiener filter. It is also noticeable that the noise reduction improved the iodine density image more than water density images, as its SSIM seems to show that the corrected image approximates the noiseless image to a higher degree.

Table 3 Whole-image SSIM value of the material density images shown in Fig. 3

Figure 3	SSIM	Figure 3	SSIM
Raw water image	0.87118	Raw iodine image	0.98003
CWF water image	0.96635	CWF iodine image	0.99597
ANW water image	0.98112	ANW iodine image	0.99803

The closer this value is to one (1), the closer the image resembles the noiseless image. The algorithm with the adaptive Wiener filter (ANW) performs better than the one using the classic Wiener filter (CWF)

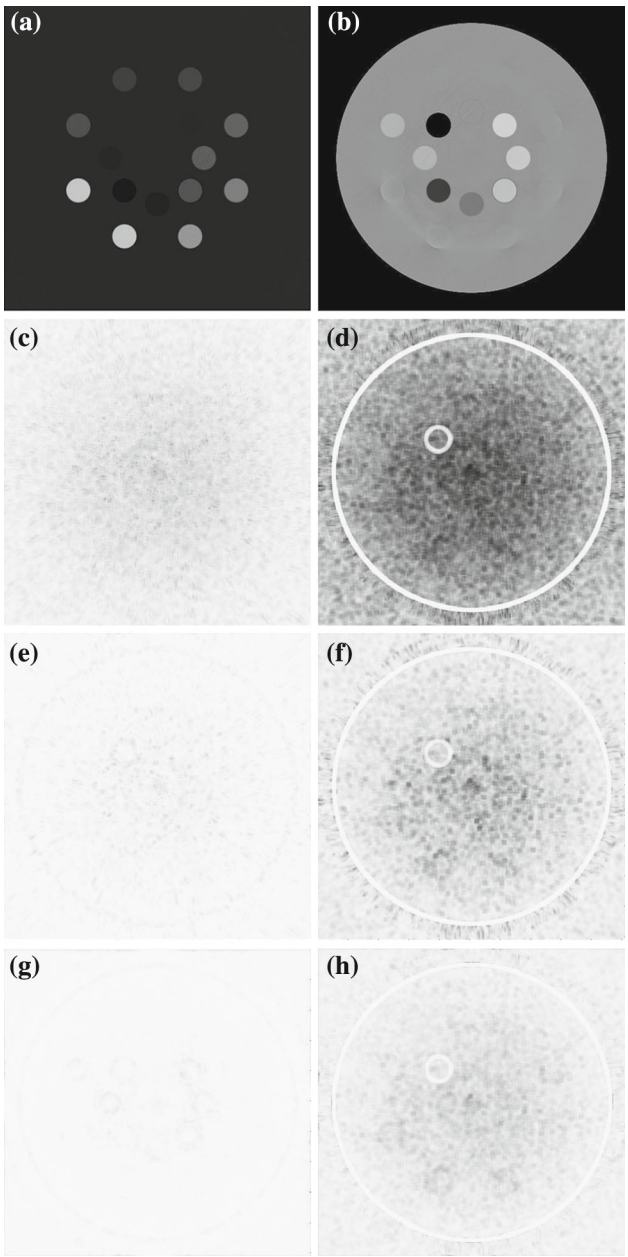

Fig. 7 Structural similarity images of Fig. 3. The whiter and more homogeneous the image is, the closer it is to the ground truth present on the leftmost column. *Darker regions* show areas where discrepancy occurs due to noise and other acquisition artifacts. **a** Noiseless iodine density image, **b** noiseless water density image, **c** SSIM of raw iodine, **d** SSIM of raw water, **e** SSIM of CWF iodine, **f** SSIM of CWF water, **g** SSIM of ANW iodine, **h** SSIM of ANW water

Discussion

Overall, both density and virtual monochromatic images that were obtained after noise correction with the adaptive Wiener

algorithm had much better defined edges and were much less noisy, with both higher CNR and SNR when compared to the raw images. The average value of a region was minimally altered, preserving valuable information that should not be altered.

However, limitations occur due to our usage of the edges from the raw VMI with minimum noise (70 keV), which does not necessarily contain all the edges from other energies. Still, the visual appearance of the images is much better and less plagued by noise.

Even though the final values of both iodine and water density images are kept as close as possible to the original images, commonly used thresholds for some specific pathologies may have to be updated. We have found that the CNR of lower-range virtual monochromatic images is not always improved. This is consistent with the results reported in Grant et al. [3], where the contrast of iodine at these low-energy levels increases less than the noise. Finally, our noise-corrected images have yet to undergo a subjective evaluation in a controlled clinical environment.

Conclusion

We have developed a new noise correction algorithm that uses an ANW filter to improve the quality of the material density images and virtual mono-chromatic images. Our algorithm's key innovations lie in (1) the usage of a customized adaptive Wiener filter, developed specifically for DECT material density images, and (2) adaptations required to keep details and avoid over-blurring of the image when combined with the anisotropic filter.

The anisotropic filter also required changes in its noise estimation function, which is more sensitive to noise than in our previous work. The algorithm is presented in an easy-to-implement work flow, and extensive quantitative analyzes were made to confirm the quality of the images after noise correction.

Compliance with ethical standards

Conflicts of interest Rafael Simon Maia, Christian Jacob, Amy K. Hara, Alvin C. Silva, William Pavlicek and J.Ross Mitchell declare that they have no conflict of interest.

References

1. Balda M, Heismann B, Hornegger J (2010) Value-based noise reduction for low-dose dual-energy computed tomography. Springer, Berlin
2. Borsdorf A, Raupach R, Flohr T, Hornegger J (2008) Wavelet based noise reduction in CT-images using correlation analysis. IEEE Trans Med Imaging 27(12):1685–1703
3. Grant KL, Flohr TG, Krauss B, Sedlmair M (2014) Assessment of an advanced image-based technique to calculate virtual monoenergetic computed tomographic images from a dual-energy examination to improve contrast-to-noise ratio in examinations using iodinated contrast media. Investig Radiol 49(9):586–592
4. Hinshaw DA, Dobbins JT III (1995) Recent progress in noise reduction and scatter correction in dual-energy imaging. In: Van Metter RL, Beutel J (eds) Medical imaging. SPIE, Washington, pp 134–142
5. Kalender W, Klotz E, Kostaridou L (1988) An algorithm for noise suppression in dual energy CT material density images. IEEE Trans Med Imaging 7(3):218–224
6. Lee JS (1980) Digital image enhancement and noise filtering by use of local statistics. IEEE Trans Pattern Anal Mach Intell 2:165–168
7. Li B, Li B, Luo J, Tang P, Mao J, Wu X (2013) Simultaneous reduction in noise and cross-contamination artifacts for dual-energy X-ray CT. BioMed Res Int 2013(6):1–8
8. Macovski A, Nishimura DG, Doost-Hoseini A, Brody WR (1983) Measurement-dependent filtering: a novel approach to improved SNR. IEEE Trans Med imaging 2(3):122–127
9. Maia RS, Jacob C, Hara AK, Silva AC, Pavlicek W, Ross MJ (2015) An algorithm for noise correction of dual-energy computed tomography material density images. Int J Comput Assist Radiol Surg 10(1):87–100
10. Park KK, Oh CH, Akay M (2011) Image enhancement by spectral-error correction for dual-energy computed tomography. In: 2011 33rd annual international conference of the IEEE engineering in medicine and biology society. IEEE, pp 8491–8494
11. Park KK, Pavlicek W, Boltz T, Paden R, Hara A, Akay M (2009) Image-based dual energy CT improvements using Gram–Schmidt method. In: Samei E, Hsieh J (eds) SPIE medical imaging. SPIE, Washington, pp 72583S–72583S-9
12. Prewitt JM (1970) Object enhancement and extraction. chap. In: Lipkin BS, Rosenfeld A (eds) Picture processing and psychopictorics. Academic Press, New York, pp 75–149
13. Rangayyan RM, Ciuc M, Faghih F (1998) Adaptive-neighborhood filtering of images corrupted by signal-dependent noise. Appl Opt 37(20):4477–4487
14. Silva AC, Lawder HJ, Hara A, Kujak J, Pavlicek W (2009) Innovations in CT dose reduction strategy: application of the adaptive statistical iterative reconstruction algorithm. Am J Roentgenol 194(1):191–199
15. Wang Z, Bovik AC, Sheikh HR, Simoncelli EP (2004) Image quality assessment: from error visibility to structural similarity. IEEE Trans Image Process 13(4):600–612
16. Warp RJ, Dobbins JT (2003) Quantitative evaluation of noise reduction strategies in dual-energy imaging. Med Phys 30(2):190–198
17. Wu X, Langan DA, Xu D, Benson TM et al (2009) Monochromatic CT image representation via fast switching dual kVp. Proc SPIE 7258:725845